A Robust Lyapunov's De-modulator for Tracking of Single/Three-Phase Grid Voltage Variables

A. K. Verma, *Member, IEEE,* C. Subramanian, *Member, IEEE,* R. K. Jarial, *Member, IEEE,* Pedro Roncero-Sánchez, *Senior Member, IEEE,* and U. Mohan Rao, *Member, IEEE*

***Abstract*—In this article, a robust Lyapunov demodulator (LD) based on orthogonal signal generation (OSG) approach for single/three-phase application is proposed. Conventionally, LD is not capable of rejecting the DC-offset in the grid signal. Thus, an additional estimation loop is required which may affect the dynamic performance. Nevertheless, an application of harmonically polluted grid voltage signal to LD may severely affect the steady-state performance of the estimated parameters. To address these issues, an enhanced LD based-OSG is proposed, wherein a moving average filter is incorporated in the LD–OSG structure. Thus, rapid rejection of DC-offset and harmonics is easily achieved without any additional loop. The proposed structure may accurately estimate the fundamental in-phase and the quadrature components. However, these orthogonal components may suffer from amplitude imbalance and errors in the phase information under off-nominal frequency conditions. Additionally, the errors in the amplitude and the phase information are eliminated using an open-loop frequency deviation detector and a feed-forward curve fitting approach. The dynamic performance of the proposed scheme has been validated by numerical and hardware studies. It is reported that, with the less sensitivity toward phase angle jump and good immunity to fundamental negative sequence, the proposed scheme is a potential technique for synchronization of single/three-phase grid connected power electronic equipment.**

***Index Terms*—Lyapunov demodulator, moving average filter (MAF), amplitude estimation, phase estimation, frequency estimation.**

I. Introduction

WITH the evolution of the smart grid, the improvement in the grid resilience and power quality relies on a good control over grid connected converters (GCCs) [1], [2]. The control architecture of GCC is composed of well known grid synchronization algorithms i.e. phase locked–loops (PLLs) and frequency locked–loops [3]–[14]. In general, an elevated performance of a control algorithm is achieved by analog or digital signal conditioning units. With the pertinent digital signal processors, the robust performance of a control technique relies on a fast removal of the noise and the harmonic components [4]. Thus, demanding the need for research on immunity based digital filtering techniques [5]. The optimized filtering techniques often applied for the developement of better control architecture of GCCs are reported in [6]–[8].

Synchronous reference frame (SRF) PLL usually provides a good estimate of the grid attributes. However, the SRF-PLL alone is incapable of handling the grid disturbances (i.e. DC-offset, harmonics and the fundamental negative sequence (FNS)). It is well known that the SRF-PLL is a type-2 system and posses low-pass filtering capability. Importantly, simultaneous rejection of the DC-offset and harmonics may impose a major challenge for the detection of the grid voltage attributes for power system applications [8]. To overcome this issue, in-loop and pre-loop filters are deployed to improve the tracking ability of the SRF-PLL [8], [9]. With the inclusion of a specific type of filtering technique, the stability margin, controller tuning, and trade-off in the response time are challenging for SRF–PLLs [10], [11]. Nevertheless, the non-adaptive pre-loop filtering methods demostrate fast dyanmic response when compared to in-loop filtering methods. However, erroneous results in the estimate of amplitude and the phase information remain challenging irrespective to the choice of control algorithm [12]. Thus, error correction units are required to achieve zero steady-state error in the estimate of the fundamental amplitude and the phase information.

It is to be recalled that the DC-offset and FNS components are the main reasons for double frequency oscillations in the estimated parameters obtained from a grid synchronization algorithm [10]–[14]. The orthgonal signal generation (OSG) filters along with an instantaneous symmetrical component method are capable of rejecting the DC-offset and FNS components [13], [14]. Thus, there is need to explore improved and accurate phase tracking algorithms with a good dynamic behavior and negligible steady-state errors accompanied by high immunity to grid disturbances.

The OSG based on demodulation of the grid voltage signal is a potential approach to estimate the grid attributes [15]–[24]. The demodulation of a single-phase signal is achieved by multiplying fixed frequency unit orthogonal signals that provide rotating reference (dq) frame components, as reported in [15], [16]. However, the presence of harmonics and DC-offset components will induce full cycle and even harmonics components in the demodulated components [16]. Thus, the least-squares-Kalman filter based demodulation approach is eqquiped with an ability to reject the negative effects of harmonics [17], [18]. Nevertheless, this approach is computationally complex owing to the higher-order finite impulse response filters. On the other hand, low pass filter (LPFs) based schemes involve in phase errors under off-nominal frequency conditions [16]–[19]. Thus, a computationally efficient infinite impulse response-LPF based demodulation scheme with minimum phase error and an improved response time is reported in [20]. The predictive filtering in conjuction with moving average filters (MAFs) may be deployed to minimize errors in the phase information [21]. On the other hand, improved frequency adaptive filtered-sequence MAF-PLL may avoid predictive filters for accurate extraction of the phase information [22]. The simplest open-loop demodulation based phase error compensation technique is reported in [23]. However, a proper rejection of the DC-offset and harmonics under off-nominal frequency condition is challenging with

this approach. Thus, a grid voltage demodulation technique as reported in [24] may be adopted with improved off-nominal harmonic and the DC-offset rejection capabilities. However, the DSC operator involved in the pre-filtering stage is responsible for elevation of the noise signal present in the grid signal. Importantly, a good dynamic response may be achieved with this technique for grid synchronization purpose. Nevertheless, the quest for improved orthogonal signal generators are still in demand. Also, the open-loop frequency estimators when combined with improved OSGs may help in attaining improved robustness, memory storage, steady-state accuracy, and dynamic performance. It is expected to have an investigation regarding the combination of new OSG structures along with the open-loop frequency estimation algorithms for achieving better accuracy and robust performance under adverse grid voltage conditions. It is well known that the open-loop frequency estimators performs well once the fundamental grid voltage signal is obtained. Thus, the pre-filters (OSGs) are responsible for strengthening the overall robustness of any synchronization scheme.

An effective approach with which to perform OSG relies on non-linear control theory [25], [26] based Lyapunov demodulation [27]–[29]. The analysis of Lyapunov based PLL (L–PLL) is reported in [27] to estimate the grid attributes. However, L–PLL is not immune to the DC-offset. To address this issue, an additional DC-offset rejection loop may be deployed with a trade-off in the response time [28], [29]. Under off-nominal frequency conditions, the improved L-PLL [29] is incapable of rejecting harmonics properly. Thus, the challenges with regard to the performance improvement are addressed, in this article, as follows: A non-adaptive enhanced Lyapunov demodulator-based-OSG (ELD–OSG) is proposed. The possibility of rejecting the DC-offset and harmonics is enhanced by incorporating MAFs in LD–OSG structure. Under off-nominal frequency conditions, steady-state errors in the estimated amplitude and phase information are eliminated through an online regression method. For this purpose, an open-loop frequency detector is considered owing to its superiority over the PLL. The salient features of the proposed scheme are as follows:

- Good immunity to harmonics, DC-offset, and FNS.
- Improved and stable dynamic behavior.
- Improved steady-state accuracy.
- Reduced tuning efforts owing to the avoidance of frequency and phase feedback loops
- Simple error compensation approach for amplitude and phase estimation.

II. Conventional Lyapunov Demodulator

The Laypunov demodulator (LD) [22] is a non-linear approach that allows to reconstruct a single-phase grid voltage signal from its $dq-$frame (i.e. direct (v_d) axis and quadrature (v_q) axis) components, as explained below:

$$\begin{aligned} v(t) &= A\,cos(\phi)\,sin(\omega_{no}t) + A\,sin(\phi)\,cos(\omega_{no}t) \\ &= v_q\,S_1 + v_d\,C_1 \end{aligned} \tag{1}$$

where, $S_1 = sin(\omega_{no}t)$, $C_1 = cos(\omega_{no}t)$, $v_q = A\,cos(\phi)$, $v_d = A sin(\phi)$, ω_{no} is the nominal angular grid frequency, and ϕ is the initial phase angle. The estimate of $v(t)$ is expressed as follows,

$$\hat{v}(t) = \hat{v}_q\,S_1 + \hat{v}_d\,C_1 \tag{2}$$

where, the estimate of the states i.e. v_q and v_d are denoted by $\hat{v}_q$ and $\hat{v}_d$, respectively. The accurate estimation of the $dq-$frame components i.e. $\hat{v}_q$ and $\hat{v}_d$ may be achieved by implementing the LD, as shown in Fig 1. The re-construction of the fundamental orthogonal signals ($\hat{v}_\alpha$ and $\hat{v}_\beta$) may be achieved by an inverse Park's Transformation (IPT).

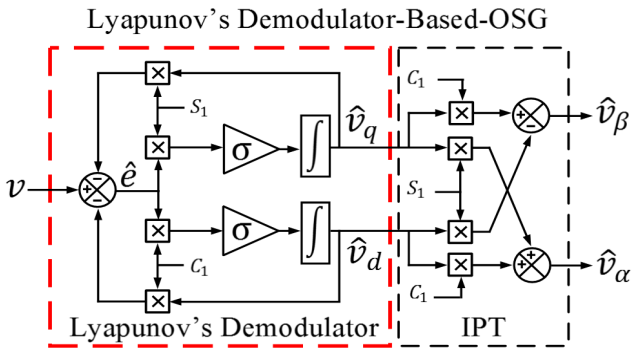

Fig. 1. General block diagram of Lyapunov's demodulator-based-OSG.

A. Lyapunov's Estimation Law

The Lyapunov's estimation law relies on the demodulation of the error ($\hat{e}$) between v and $\hat{v}$ which is given below:

$$\dot{\hat{v}}_q(t) = \sigma\,sin(\omega_{no}t)\,(v - \hat{v}) = \sigma\,sin(\omega_{no}t)\,\hat{e} \tag{3}$$

$$\dot{\hat{v}}_d(t) = \sigma\,cos(\omega_{no}t)\,(v - \hat{v}) = \sigma\,cos(\omega_{no}t)\,\hat{e} \tag{4}$$

where, the time derivatives of state variables (v_q and v_d) are $\dot{\hat{v}}_q$ and $\dot{\hat{v}}_q$, respectively and σ represents a constant gain. The generalized state space model is expressed as follows,

$$\dot{\hat{x}} = \sigma\,\mathbf{H}\,\hat{e} \tag{5}$$

$$\hat{v} = \mathbf{H}^T\,\hat{x} \tag{6}$$

where, $\mathbf{H} = [sin(\omega_{no}t),\ cos(\omega_{no}t)]^T$ and $\hat{x} = [\hat{v}_q,\ \hat{v}_d]^T$.

B. Stability and Convergence of State-Space Vector

As reported in [25], [26], and [28], the stability of the Lyapunov estimation law is based on Kalman-Yakubovich-Popov and Meyer-Kalman-Yakubovich Lemmas along with the strictly positive real Lyapunov design approach. Thus, the appropriate choice of Lyapunov like function (V_{LP}) is when the time derivative of V_{LP} is non-positive, i.e. $\dot{V}_{LP} \leq 0$. This ensures guaranteed boundedness as well as the stability $(\hat{e}, \hat{x}, \dot{\hat{x}})$ as per [25]. In addition, the signal vector $\mathbf{H}$ follows the persistent excitation (PE) property if there exist α_o, α_1, and $T_o > 0$ such that,

$$\alpha_1 I \geq \int_t^{t+T_o} \mathbf{H}(\tau)\mathbf{H}^T(\tau)d\tau \geq \alpha_o I \tag{7}$$

Thus, unboundedness of signal vector $\mathbf{H}$ is not the case for Lyapunov estimation law [25], [28]. In the time interval $[t, t+T_0]$, the integral of the matrix $\mathbf{H}(\tau)\mathbf{H}^T(\tau)$ is uniformly positive definite [25], [26]. Hence, the exponential convergence of $\hat{x}$ to x is ensured.

III. Proposed Enhanced LD–OSG based Scheme

In this section, the analysis of the proposed enhanced LD (ELD) based OSG is investigated for single/three-phase grid attributes tracking. The major challenges with regard to the elimination of DC-offset and the harmonics are discussed. Under off-nominal frequency deviations, the steady-state output of ELD–OSG will be erroneous in regard to the fundamental amplitude and phase angle information. Thus, a computationally efficient open-loop estimation of the frequency deviation is presented to eliminate the aforementioned errors.

A. Error Boundedness

As discussed, the error term in (3) and (4) may be expressed as follows:

$$\hat{e} = v - \hat{v} = v_q\, S_1 + v_d\, C_1 - \hat{v}_q\, S_1 - \hat{v}_d\, C_1 \tag{8}$$

The errors in the estimation may be represented as follows:

$$\bar{v}_q = v_q - \hat{v}_q \tag{9}$$

$$\bar{v}_d = v_d - \hat{v}_d \tag{10}$$

Substituting (9) and (10) in (8), the error ($\hat{e}$) is,

$$\hat{e} = \bar{v}_q\, S_1 + \bar{v}_d\, C_1 \tag{11}$$

Thus, a Laypunov's like function is constructed as follows:

$$V_{LP}(t) = \frac{\bar{v}_q^2(t) + \bar{v}_d^2(t)}{2} \tag{12}$$

The time derivative of (12) yields.

$$\dot{V}_{LP}(t) = \bar{v}_q \dot{\bar{v}}_q + \bar{v}_d \dot{\bar{v}}_d \tag{13}$$

where, $\dot{\bar{v}}_q = -\dot{\hat{v}}_q$ and $\dot{\bar{v}}_d = -\dot{\hat{v}}_d$. Similarly, the time derivative of estimation errors may be expressed as follows:

$$\dot{\bar{v}}_q = -\sigma S_1 \hat{e} \tag{14}$$

$$\dot{\bar{v}}_d = -\sigma C_1 \hat{e} \tag{15}$$

Thus, $\dot{V}_{LP}(t)$ may be rewritten as follows:

$$\dot{V}_{LP}(t) = -\sigma\, (\bar{v}_q\, S_1 + \bar{v}_d\, C_1)\, \hat{e} = -\sigma\, \hat{e}^2 \tag{16}$$

According to PE property [25],[26], for positive values of $\sigma > 0$, $\dot{V}_{LP}(t) \leq 0$ must hold. Thus, it may be concluded that,

$$\lim_{t\to\infty} = \hat{v}_q = v_q \tag{17}$$

$$\lim_{t\to\infty} = \hat{v}_d = v_d \tag{18}$$

From (17) and (18), the unknowns v_q and v_d are estimated without any steady-state error.

B. Effect of the DC-Offset

The Lyapunov's estimation law is sensitive to DC-offset component present in the grid signal, as discussed in [28], [29]. In order to deal with this issue, a third state may be added representing the DC-offset ($\hat{V}_o$) [28]. In addition, a constant element i.e. 1 is added to the signal vector (**H**) as $\mathbf{H} = [sin(\omega_{no}t),\ cos(\omega_{no}t),\ 1]^T$ and a tuning gain σ_1 may be introduced to update the law for rejection of DC-offset, as reported in [29]. In Fig. 2, the implementation of the DC-offset rejection loop is depicted. From [28], [29], the suitable choice for σ and σ_1 is, $\sigma = 8f_{no}$ and $\sigma_1 = f_{no}$ where, f_{no} is the nominal frequency i.e. 50 Hz. As $\sigma_1 = \sigma/8$, it is understood that the convergence rate of $\hat{V}_o$ state may affect the overall dynamic response. Thus, a grid voltage signal contaminated with a DC-offset is considered as follows:

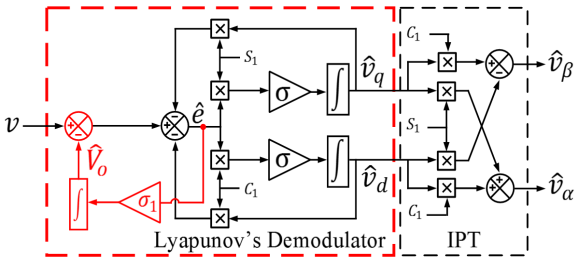

Fig. 2. Implementation of DC-offset rejection loop.

$$v(t) = A\, sin(\omega_{no}t + \phi) + V_o = v_q\, S_1 + v_d\, C_1 + V_o \tag{19}$$

Using (8) and (19), the error ($\hat{e}_1$) in case of a DC-offset is,

$$\hat{e}_1 = \hat{e} + V_o = v_q\, S_1 + v_d\, C_1 - \hat{v}_q\, S_1 - \hat{v}_d\, C_1 + V_o \tag{20}$$

Using (3) and (4), $\hat{e}_1$ may be demodulated to obtain $\dot{\hat{v}}_q$ and $\dot{\hat{v}}_d$ in terms of $\hat{e}$ and V_o as shown below:

$$\dot{\hat{v}}_q = \sigma S_1 \hat{e}_1 = \sigma\, S_1\, \hat{e} + \sigma\, V_o\, S_1 \tag{21}$$

$$\dot{\hat{v}}_d = \sigma C_1 \hat{e}_1 = \sigma\, C_1\, \hat{e} + \sigma\, V_o\, C_1 \tag{22}$$

From (21) and (22), it may be observed that V_o will become a full cycle component with an oscillating frequency of f_{no}. To deal with this issue, a moving average filter (MAF) [10], [21] may be deployed in LD–OSG structure, as shown in Fig. 3. The window length (T_w) of MAF is equivalent to one

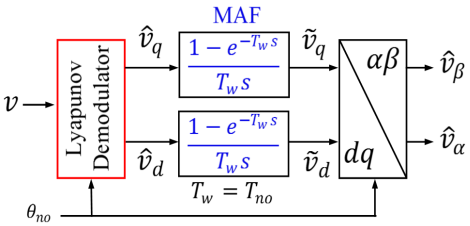

Fig. 3. Improved orthogonal signal generation based on LD.

fundamental period i.e. $T_w = T_{no}$, where $T_{no} = 1/f_{no}$ and $f_{no} = 50$ Hz. In Fig. 3, the filtered dq-frame components i.e. $\tilde{v}_q$ and $\tilde{v}_d$ are fed to IPT to obtain $\hat{v}_\alpha$ and $\hat{v}_\beta$. In order to understand the effect of MAF in the ELD–OSG structure, a frequency response plot is provided in Fig. 4.

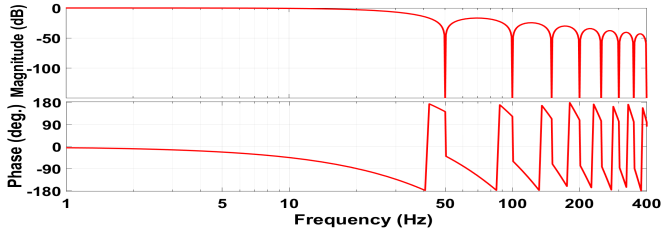

Fig. 4. Frequency response plot for ELD-based-OSG.

It may be observed that the proposed structure behaves as a comb filter which may effectively reject the DC-offset component. In a simulation environment, the fundamental amplitude (i.e. $\hat{A} = \sqrt{\hat{v}_\alpha^2 + \hat{v}_\beta^2}$) is estimated in the presence of 10% DC-offset with 50% voltage sag in the grid signal, as shown in Fig. 5. It may be observed that the ELD–OSG structure posses

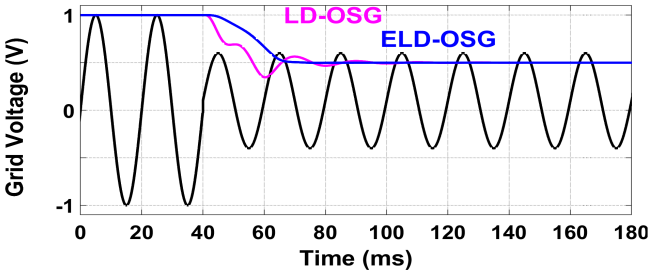

Fig. 5. Dynamic performance comparison in case of a DC-Offset in grid signal.

a good DC-offset rejection capability and takes approximately two times of fundamental cycle (i.e. 40 ms) to estimate the amplitude. The ELD–OSG structure demonstrates good and stable dynamic performance as compared to the LD–OSG structure.

C. Small Signal Model and Effect of Harmonics

In this section, the small signal model of the LD is revisited to explore the type of filtering capability associated with the LD, as shown in Fig. 6 wherein D_1 denotes the output disturbance.

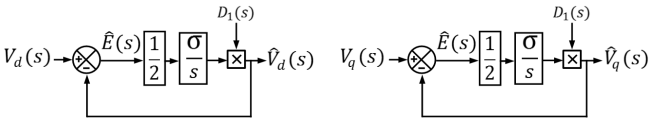

Fig. 6. Small signal model of the LD.

It may be inferred that the error term is subdivided into two equal parts between the input states (v_d and v_q) to the output states ($\hat{v}_d$ and $\hat{v}_q$). The simplified transfer function relationship is as follows,

$$\frac{\hat{V}_d(s)}{V_d(s)} = \frac{1}{\left(\frac{s}{\omega_c}\right) + 1} \tag{23}$$

$$\frac{\hat{V}_q(s)}{V_q(s)} = \frac{1}{\left(\frac{s}{\omega_c}\right) + 1} \tag{24}$$

where, $\omega_c = \sigma/2$ is the cut-off frequency. The choice of σ will affect the low pass filtering capability of the Lyapunov demodulator, as shown in Fig. 7. It is observed that for $\sigma \geq 500$ may lead to large overshoots in the estimate of the fundamental amplitude. In addition, the steady-state estimation error (p.u.) in the estimated amplitude in the presence of harmonics may increase. Thus, the suitable choice of σ may lie in the range of $400 \leq \sigma \leq 600$ with a trade-off in the response time and harmonic rejection ability. To further enhance the harmonic rejection capability of the LD–OSG

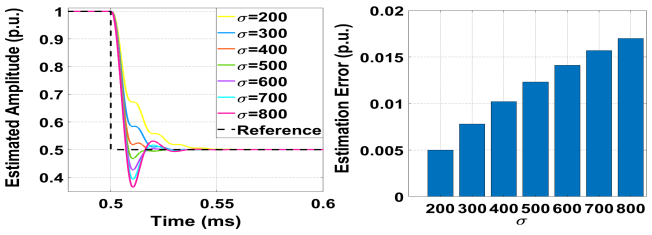

Fig. 7. The Step response and the error in presence of harmonics in the amplitude estimation for different values of σ.

structure, the MAF filter is essential. To understand this fact, a third harmonic and the fundamental component are considered in the grid voltage signal as follows:

$$\begin{aligned} v(t) &= A\, sin(\omega_{no} t + \phi) + v_3(t) \\ &= v_q\, S_1 + v_d\, C_1 + A_3\, sin(3\,\omega_{no}\, t + \phi_3) \end{aligned} \tag{25}$$

where, A_3 and ϕ_3 are the amplitude and the phase of the third harmonic component, respectively. Similar to (21) and (22), for the third harmonic case, the state variables may be re-written as follows:

$$\dot{\hat{v}}_q = \sigma\, S_1\, \hat{e} + \sigma \underbrace{v_3(t)\, sin(\omega_{no} t)}_{A} \tag{26}$$

$$\dot{\hat{v}}_d = \sigma\, C_1\, \hat{e} + \sigma \underbrace{v_3(t)\, cos(\omega_{no} t)}_{B} \tag{27}$$

The terms 'A' and 'B' can be rewritten as follows:

$$v_3(t)\, sin(\omega_{no} t) = \frac{A_3}{2}[cos(2\,\omega_{no}\, t) - cos(4\,\omega_{no}\, t)] \tag{28}$$

$$v_3(t)\, sin(\omega_{no} t) = \frac{A_3}{2}[sin(2\,\omega_{no}\, t) + sin(4\,\omega_{no}\, t)] \tag{29}$$

It may be inferred that, $\hat{v}_q$ and $\hat{v}_d$ are affected by double frequency and even-harmonic components. From Fig. 4, it is important to note that the inclusion of MAF will ensure good rejection of even harmonic components. In Fig. 8, each 5% of 3^{rd}, 5^{th}, and 7^{th} harmonics in conjunction with a 50% voltage sag are considered in the grid signal. It may be

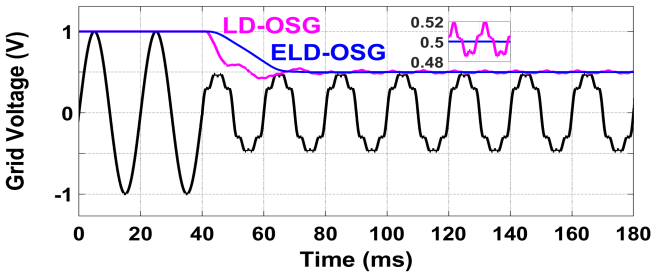

Fig. 8. Performance comparison in case of harmonics in the grid signal.

observed that the ELD-OSG and the LD-OSG can track the amplitude change. However, LD–OSG is less immune against harmonics in the grid signal. Nevertheless, the ELD–OSG does not suffer from steady-state oscillations without compromising the response time.

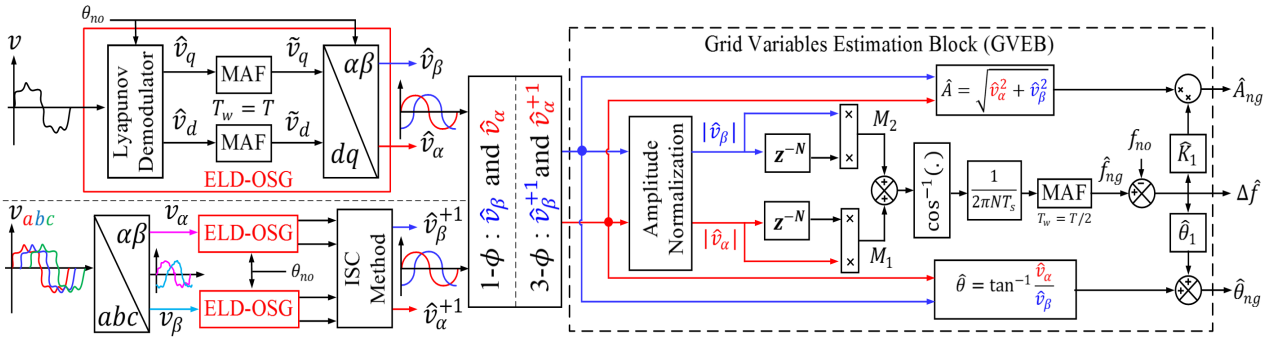

Fig. 9. Schematic diagram for the proposed single/three-phase scheme with GVEB.

D. Discrete time realization of ELD–OSG

The discrete time derivative of the state variables may be expressed as follows:

$$\hat{v}_q(k) - \hat{v}_q(k-1) = \sigma\, S_1\, \hat{e}\, T_s \tag{30}$$

$$\hat{v}_d(k) - \hat{v}_q(k-1) = \sigma\, C_1\, \hat{e}\, T_s \tag{31}$$

where, the sampling period and the current sampling instant are T_s and k, respectively. Certainly, this simple structure resolves algebraic loop issues as the estimated states are fed-back similarly to a closed loop system. Thus, a unit delay based simple infinite impulse response-integrator [31] may be deployed. Thereby, a modified gain is $\hat{\sigma} = \sigma T_s = 8 f_{no} T_s$ where, $f_{no} = 50$ Hz. The discrete time architecture of the ELD–OSG is depicted in Fig. 10. Moreover, the error in

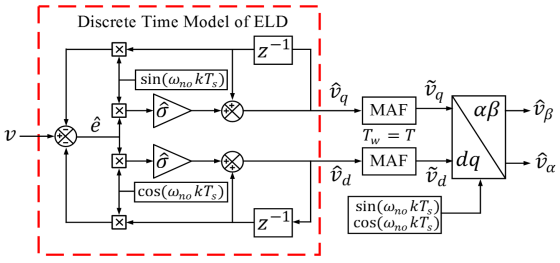

Fig. 10. Alternative discrete time structure of ELD-OSG.

the output of the ELD–OSG structure are expected under off-nominal frequency conditions. Hence, the estimation of the fundamental amplitude and the phase information will be inaccurate.

E. Estimation of the Deviation in Frequency

The steady-state error in the estimated amplitude and phase are caused due to deviations in the fundamental frequency. In the proposed work, the deviation in frequency may be estimated from two consecutive samples of the $\hat{v}_\alpha$ and $\hat{v}_\beta$, as follows:

$$M_1 = |\hat{v}_\alpha(k)| * |\hat{v}_\alpha(k-N)| \tag{32}$$

$$M_2 = |\hat{v}_\beta(k)| * |\hat{v}_\beta(k-N)| \tag{33}$$

where, $|\hat{v}_\alpha|$, $|\hat{v}_\beta|$ are the normalized orthogonal signals and N is the distance between two consecutive samples (i.e. $N = 30$ [24]). Adding (32) to (33), the estimated grid frequency ($\hat{f}_{ng}$) is computed as follows:

$$cos\,(N\,\hat{\omega}_{ng} T_s) = M_1 + M_2 \tag{34}$$

$$\hat{f}_{ng} = \frac{\hat{\omega}_{ng}}{2\pi} = \frac{1}{2\pi N T_s} cos^{-1}(M_1 + M_2) \tag{35}$$

where, $\hat{\omega}_{ng}$ is the estimated angular grid frequency. The estimation of the deviation in frequency is,

$$\Delta\hat{f} = \hat{f}_{ng} - f_{no} \tag{36}$$

where, f_{no} is the nominal frequency. In addition, the application of the proposed ELD–OSG scheme for single-phase and three-phase schemes with a common grid variables estimation block (GVEB) is exemplified in Fig. 9. In a three-phase scheme, the two individual blocks are deployed to the decoupled orthogonal signals obtained from Clarke's transformation. Thereby, the fundamental positive sequence components ($\hat{v}_\alpha^{+1}$ & $\hat{v}_\beta^{+1}$) are extracted by applying the instantaneous symmetrical component (ISC) method [24].

F. Estimation of Amplitude and Phase with Correction

In this section, amplitude and phase corrections are carried out for single and three-phase grid voltage monitoring. For the single-phase case, the estimated amplitude is,

$$\hat{A} = \sqrt{\hat{v}_\alpha^2 + \hat{v}_\beta^2} \tag{37}$$

For the three-phase case, the estimated amplitude is,

$$\hat{A} = \sqrt{(\hat{v}_\alpha^{+1})^2 + (\hat{v}_\beta^{+1})^2} \tag{38}$$

Equations (37) and (38) are the feasible solutions under nominal frequency conditions. However, when the grid frequency deviates from its nominal value, then the output of the ELD–OSG suffers from amplitude imbalance in $\hat{v}_\alpha$ and $\hat{v}_\beta$. To address this issue, a ratio of the per unit amplitude to $\hat{A}$ may be defined,

$$\hat{K}_1 = \frac{1}{\hat{A}} \tag{39}$$

Hereafter, the supply frequency is varied in steps from 47-52 Hz i.e. 1 Hz step-size then $\hat{K}_1$ is computed offline, as shown in Table I. Once $\Delta\hat{f}$ is known from (36) then a quadratic curve

TABLE I
SIMULATED DATA FOR AMPLITUDE AND PHASE CORRECTION FACTOR

Δf (Hz)	-3	-2	-1	0	1	2
$\hat{\theta}_1$ (rad.)	-0.2255	-0.141	-0.0572	0.0262	0.1092	0.192
$\hat{K}_1$	0.9768	0.9829	0.990786	1	1.0107	1.0231

fitting method is applied online to update $\hat{K}_1$ as follows:

$$\hat{K}_1 = 0.0008\,(\Delta\hat{f})^2 + 0.01\,(\Delta\hat{f}) + 1 \tag{40}$$

The correct estimated amplitude (A_{ng}) is,

$$\hat{A}_{ng} = \hat{K}_1\sqrt{\hat{v}_\alpha^2 + \hat{v}_\beta^2} = \hat{K}_1\hat{A} \tag{41}$$

From (41), it can be inferred that if $\hat{A}$ is compensated correctly, then $\hat{A}_{ng} \to 1$. Similarly, the phase angle information for the single-phase case is estimated as follows:

$$\hat{\theta} = \arctan\left(\frac{\hat{v}_\alpha}{\hat{v}_\beta}\right) \tag{42}$$

For the three-phase case, the estimated phase is,

$$\hat{\theta} = \arctan\left(\frac{\hat{v}_\alpha^{+1}}{\hat{v}_\beta^{+1}}\right) \tag{43}$$

The error in the phase information is denoted by $\hat{\theta}_1$ which may be obtained by subtracting the artificially generated ramp phase angle (θ_t) from $\hat{\theta}$ i.e. $\hat{\theta}_1 = \theta_t - \hat{\theta}$. Similar to the procedure followed in the amplitude correction case, for every step change in the supply frequency $\hat{\theta}_1$ is noted offline, as shown in Table I. Using (36), $\hat{\theta}_1$ is expressed in terms of $\Delta\hat{f}$ which may be updated through an online linear regression method as expressed below:

$$\hat{\theta}_1 = 0.0835(\Delta\hat{f}) + 0.0257 \tag{44}$$

The actual phase angle information is,

$$\hat{\theta}_{ng} = \hat{\theta} + \hat{\theta}_1 \tag{45}$$

It may be understood that, if $\hat{\theta}$ is correctly compensated then $\hat{\theta}_{ng} \to \theta_t$. Similarly, the correction factors for the three-phase case in GVEB remain unchanged as shown in Fig. 9, only the filter configuration needs to be changed.

IV. NUMERICAL RESULTS

The performance of the proposed ELD–OSG scheme is compared with LD–PLL [29] in MATLAB/ Simulink environment. The simulation parameters are as follows: 1) grid voltage: 1 p.u., 50 Hz, and sampling frequency of 12 kHz; 2) LD–PLL: $\sigma = 400$, $\sigma_1 = 50$, $k_p = 5000$; and 3) ELD–OSG scheme: $\sigma = 600$ thus $\hat{\sigma} = 0.05$ and $N = 30$. The following two test cases are considered: 1) single-phase (off-nominal condition) and three-phase (unbalance, unequal DC-offset, and frequency drift).

A. $1-\phi$: *Frequency Step with DC-offset, and Harmonics*

For the single-phase ($1-\phi$) case: total harmonic distortion (THD) of 10.67% as per European standard i.e EN501060 [30] is considered in the grid signal, as given in Table II. In the corresponding waveform as shown in Fig. 11, the grid signal is subjected to a 10% DC-offset and a frequency jump of +2 Hz. It could be observed that the proposed ELD–OSG

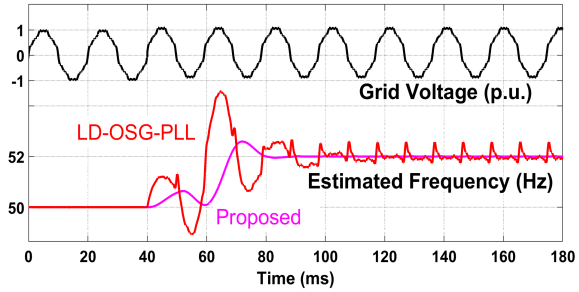

Fig. 11. Estimation of frequency in presence of DC-offset, frequency step, and harmonics.

scheme takes approximately 50 ms to estimate the frequency with good immunity to DC-offset and harmonics. The LD-PLL suffers from large overshoots and poor dynamic performance as compared to the proposed scheme.

B. $3-\phi$: *Unbalance, Unequal DC-offset, and Frequency Drift*

For the three-phase ($3-\phi$) case: A frequency step of +2 Hz along with 0.3 p.u. fundamental negative sequence component (FNS) and an unequal DC-offset (0.1, 0.2, and 0.3 p.u per phase) in the grid signal are considered, as shown in Fig. 12. Both, the LD–PLL and the proposed scheme has

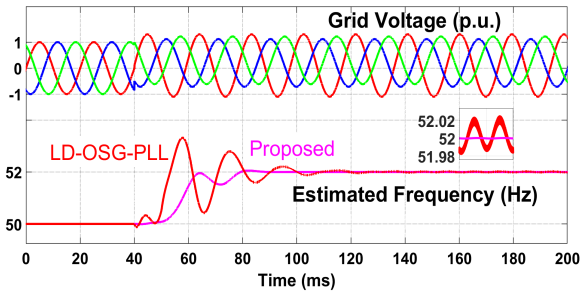

Fig. 12. Fequency estimation in presence of the FNS, Unequal DC-offset, and frequency step.

good frequency tracking ability. However, LD–PLL suffers from large transients and steady-state oscillations. Moreover, both the schemes are capable of rejecting the FNS component.

V. EXPERIMENTAL RESULTS

The experimental validation is considered based on dSPACE 1104 controller board and the estimated parameters are cap-

TABLE II
HARMONICS IN THE GRID SIGNAL AS PER EN 50160 STANDARD

Order	3	5	7	9	11	13	15	17	THD
%	5	6	5	1.5	3.5	3	0.5	2	10.67

tured on a 16 channel scopecorder (DL-750). The performance of the ELD–OSG scheme is compared with the LD–PLL [29]. The experimental parameters for the algorithms are similar to the numerical results. To understand the significance of the ELD–OSG, a single-phase and a three-phase variant of the proposed ELD–OSG scheme are provided. Importantly, two critical test conditions are considered for single and three-phase case. Thereby, the dynamic performance improvement may be observed at nominal and off-nominal frequency conditions.

A. Single-Phase Case

The grid voltage signal with a THD of 10.67% is subjected to two critical test conditions as follows:

1. 50% voltage sag, 10% DC-offset, 30° phase transition and harmonics at nominal frequency condition i.e. 50 Hz, as shown in Fig. 13.

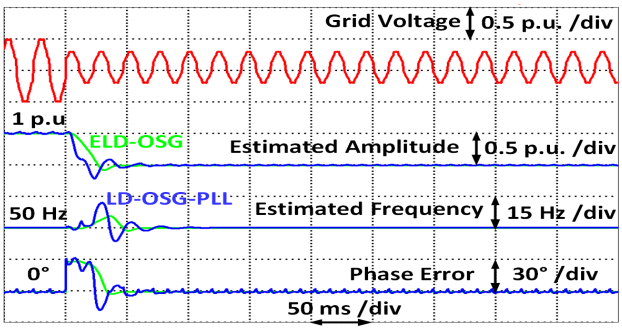

Fig. 13. $1-\phi$ estimation of the fundamental grid attributes at nominal frequency condition.

2. Frequency jump of +2 Hz (i.e. 50-52 Hz), 10% DC-offset and harmonics, as depicted in Fig. 14.

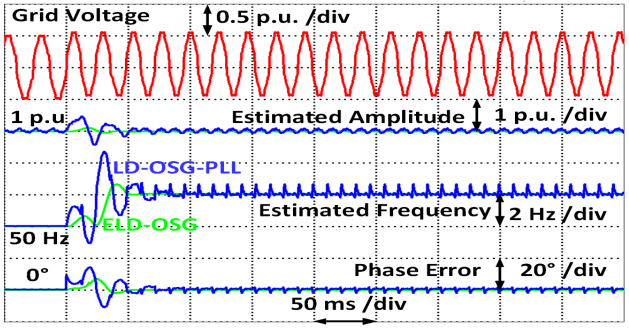

Fig. 14. $1-\phi$ off-nominal frequency tracking ability in presence of DC-offset and harmonics.

In Fig. 13, it may be observed that the proposed scheme takes approximately 2.5 times of fundamental cycle to estimate the grid parameters. In addition, the phase angle jump leads to a peak overshoot in the estimated frequency i.e. 3 Hz and 12.5 Hz for the ELD–OSG scheme and the LD–PLL, respectively. Under off-nominal frequency conditions (Fig. 14), the proposed scheme posses a better harmonic rejection capability as compared to LD–PLL. It is evident that both the schemes are capable of rejecting the DC-offset component. However, the dynamic performance of the LD–PLL is more oscillatory when compared to the ELD–OSG scheme. The peak overshoot in frequency and phase information, for the LD–PLL is 2.57 Hz and 18° whereas for the ELD–OSG scheme is 0.6 Hz and 11°. Moreover, the ELD–OSG scheme posses negligible amount of steady-state ripples in the estimated quantities. Thus, a robust performance is achieved with the ELD–OSG scheme for its suitability in single-phase applications.

B. Three-Phase Case

The occurrence of grid fault may cause voltage unbalance, as a consequence a FNS component may arise. Simultaneously, the presence of unequal DC-offset (0.1, 0.2, and 0.3 p.u. per phase) and harmonics (each 5% of 5^{th} and 7^{th}, 3% of 11^{th} and 1% of 13^{th}) in the grid may hinder the performance of the synchronization algorithm. Thus, two severe test conditions in this case are as follows:

1. Symmetrical 50% voltage sag, unequal DC-offset, phase angle transition of 30°, and harmonics at nominal frequency condition, as shown in Fig. 15.

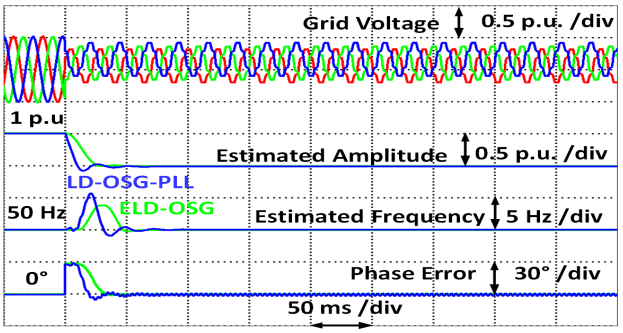

Fig. 15. $3-\phi$ estimation of the fundamental grid attributes at nominal frequency condition.

2. The FNS of 0.3 p.u., frequency step of +2 Hz (i.e. 50-52 Hz), an unequal DC-offset, and harmonics, as depicted Fig. 16.

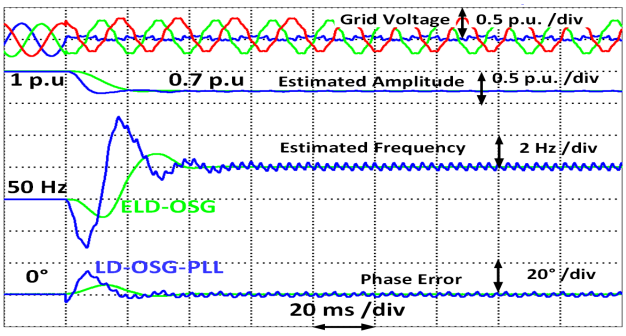

Fig. 16. $3-\phi$ off-nominal frequency tracking ability in presence of DC-offset, FNS, and harmonics.

In Fig. 15, the settling time performance of the ELD–OSG scheme and the LD-PLL are approximately 50 ms and 55 ms, respectively. However, the overshoot in frequency is 3 Hz and 8.9 Hz for the ELD–OSG scheme and the LD–PLL, respectively. In Fig. 16, by reducing the magnitude of phase 'a'

to 0.1 p.u., a 0.3 p.u. FNS is developed. The filter configuration of the three-phase ELD-OSG scheme and the three-phase LD-PLL are implemented as suggested in Fig. 9. It may be observed that, both the schemes are capable of rejecting the FNS component. However, a slower dynamic performance is observed in case of the LD–PLL. The peak overshoot in the frequency and the phase information, for the LD–PLL is 3 Hz and 18° whereas for the ELD–OSG scheme is 0.8 Hz and 10°. Also, the maximum steady-state errors in amplitude and phase are 0.0015 p.u. and 0.1 °, respectively. The relative frequency error is well below 0.03% mentioned in IEC Standard 61000-4-7 [32], as exemplified in Fig. 17.

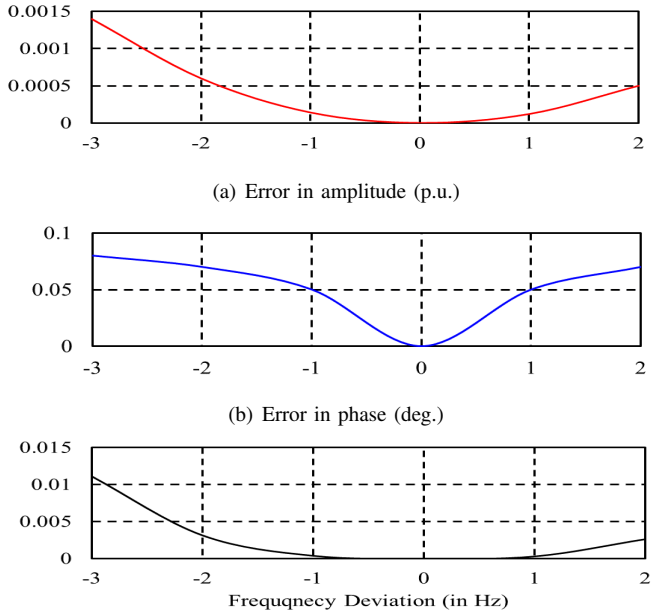

(a) Error in amplitude (p.u.)

(b) Error in phase (deg.)

(c) Relative frequency error (Hz)

Fig. 17. Steady-state error in amplitude, phase, and frequency.

Hence, the ELD–OSG scheme has good immunity to DC-offset and harmonics under off-nominal frequency conditions.

C. Results and discussion

A summary of the experimental results for single/three-phase test cases are presented in Table III. The peaks errors in the estimated fundamental amplitude, phase, and frequency information are denoted by ΔA_p, Δf_p, and $\Delta\theta_p$. The settling time performance is denoted by t_r. It is understood that the proposed scheme takes ≈2.5 times of the fundamental period to estimate the grid parameters. With help of the MAF filter, a higher immunity to the negative effect of DC-offset and harmonics is attained. The phase angle transition affects the frequency information in both the LD–PLL and the ELD–OSG. However, a maximum overshoot of 3 Hz is observable in the estimated frequency in the case of the proposed scheme. Moreover, the proposed three-phase scheme has demonstrated a good FNS and DC-offset rejection capability with a net response time of ≈50 ms. Thus, the proposed scheme has good potential for detection of selective harmonic and fundamental grid voltage attributes.

TABLE III
SUMMARY OF COMPARATIVE PERFORMANCE EVALUATION

Case	Peak Errors	$1-\phi$		$3-\phi$	
		ELD–OSG	LD–PLL	ELD–OSG	LD–PLL
Voltage Sag	ΔA_p (p.u.)	-	-	-	-
	Δf_p (Hz)	3	12.5	3	8.9
	$\Delta\theta_p$ (°)	-	-	-	-
	t_r (ms)	≈50	≈55	≈50	≈55
Frequency Step	ΔA_p (p.u.)	0.06	0.11	-	-
	Δf_p (Hz)	0.6	2.57	0.8	3
	$\Delta\theta_p$ (°)	11	18	10	18
	t_r (ms)	≈50	≈55	≈50	≈55
DC-offset Rejection		Yes	Yes	Yes	Yes
Harmonic Attenuation		Good	Poor	Good	Poor
Steady-State Accuracy		High	Low	High	Low
FNS Rejection		-	-	Yes	Yes
Control parameters		2	3	2	3

D. Application: Harmonic Parameter Estimation

In Fig. 18, the information of $\hat{K}_1$, $\hat{\theta}_{ng}$ and N is essential to accurately extract the amplitude and the phase information of a harmonic component. Thus, a linear interpolation method (LIM) [19] is deployed for the determination of N value. The frequency adaptive ELD-OSG module is then subjected

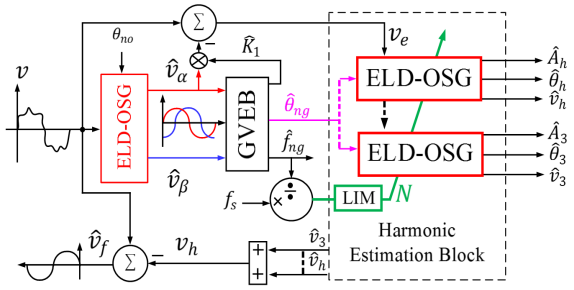

Fig. 18. Estimation of harmonic parameters.

to an error signal $v_e = v - \hat{v}_\alpha$. In addition, individual block of the ELD-OSG structure is tuned to $h * \hat{\theta}_{ng}$, where $h = 3, 5, 7, 9, ..2L+1$, $L \geq 0 \in I$ in the harmonic estimation block. Thereby, the amplitude and phase information is computed through $\hat{A}_h = \sqrt{\hat{v}_{h\alpha}^2 + \hat{v}_{h\beta}^2}$ and $\hat{\theta}_h = tan^{-1}(\hat{v}_{h\alpha}/\hat{v}_{h\beta})$, respectively. Hence, the fundamental component (i.e. $\hat{v}_f$) may be effectively extracted by subtracting the estimated harmonic components ($v_h = \sum_{h=3,5,7,9..}^{L} \hat{v}_h$). In Fig. 19, each 5% of

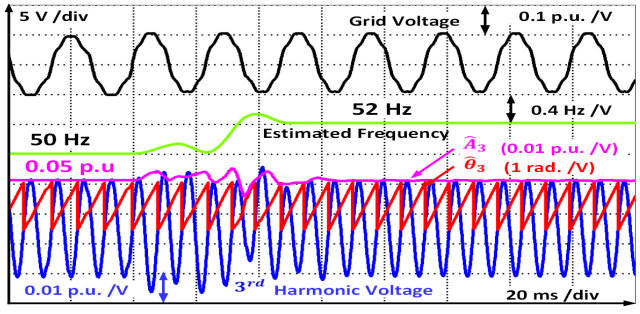

Fig. 19. Estimation of third harmonic component in the presence of DC-offset and frequency step of +2Hz.

3^{rd}, 5^{th}, 7^{th}, and DC-offset along with a step change of +2 Hz in the supply frequency are considered in the grid signal. It may be observed that the third harmonic component is accurately estimated within 2.5 times of the fundamental cycles.

E. Comparison with Other Synchronization Schemes

In this section, a comparative performance evaluation of the proposed scheme with the existing solutions is provided. The comparison is made with respect to an improved open-loop scheme (IOLS) [23], the double second order generalized integrator (DSOGI)-PLL [12], and the MAF-PLL [11]. The case studies are considered under nominal and off-nominal frequency conditions. In Fig. 20, grid voltage is subjected to 120° phase jump along at 50 Hz. In Fig. 20(a), in the absence of DC-offset the IOLS has outperformed in the ability of tracking the estimated phase without any steady-state error. It

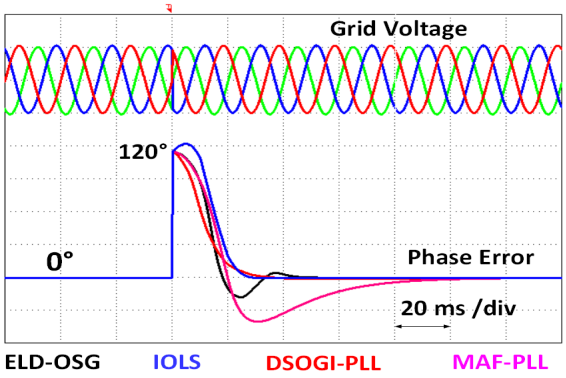

(a) 120° phase jump without DC-offset

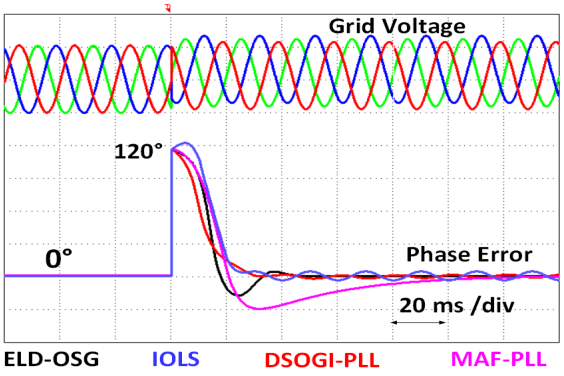

(b) 120° phase jump with unequal DC-offset

Fig. 20. Comparative phase angle tracking performance.

is to be noticed that the proposed scheme has good capability in tracking the estimated phase as compared to MAF–PLL and DSOGI–PLL. In phase jump case, the proposed scheme is comparatively more immune to the DC-offset similar to MAF-PLL while adhering a good dynamic response. On the other hand, the ELD–OSG scheme has better capabilities to reject the DC-offset component when compared to IOLS and DSOGI–PLL, as shown in Fig. 20(b). Subsequently, off-nominal frequency tracking ability of IOLS shall be faster than other schemes as ensured by the previous test case and confirmed in Fig. 21(a). However, the MAF–PLL, DSOGI–PLL, and IOLS still suffers from steady-steady oscillations when compared to ELD–OSG scheme. Further, IOLS and

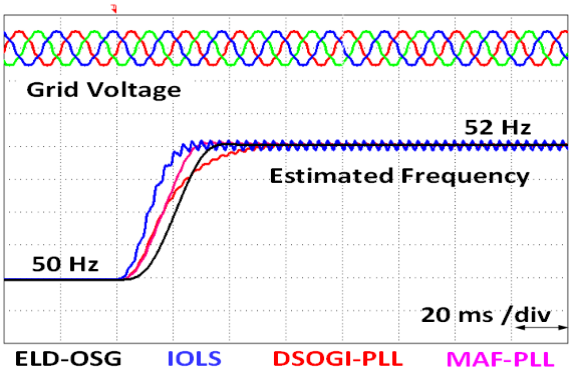

(a) +2 Hz frequency step without DC-offset

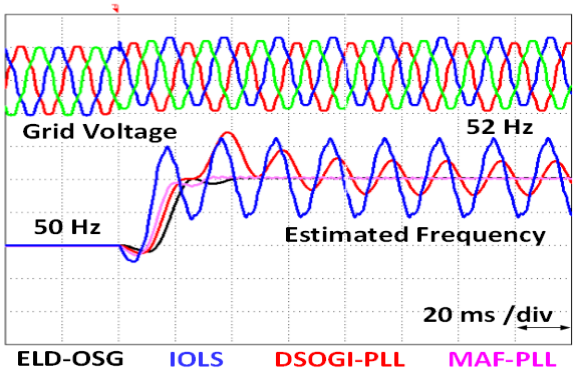

(b) +2 Hz frequency step with DC-offset

Fig. 21. Comparative frequency step (50-52 Hz) tracking performance in presence of harmonics and DC-offset

DSOGI–PLL are incapable of rejecting the unequal DC-offset component present in the grid signal, as shown in Fig. 21(b). Moreover, the ELD–OSG scheme suffers from a negligible amount of steady-state error as compared to MAF–PLL.

VI. Conclusion

A robust and improved Lyapunov demodulator based non-linear filtering technique is proposed for tracking the single/three-phase fundamental grid voltage attributes. An enhanced DC-offset and harmonic rejection capability is achieved by deploying MAF in the ELD–OSG structure. In effect of which no additional feed-back loop is required to reject the DC-offset. Under off-nominal frequency conditions, the output of the ELD–OSG filter is erroneous. Thus, feed-forward compensation method dependent on open-loop frequency deviation technique is a rescuer for the elimination of errors in the amplitude and the phase information. However, the amplitude imbalance will not affect the estimate of the fundamental frequency (i.e. ≈2.5 times of fundamental period). From experimental measurements, it can be inferred that the proposed scheme is found less sensitive towards phase angle jump as compared to the LD–PLL. Nevertheless, the proposed three-phase scheme outperformed in respect to stable and dynamic performance abilities. In addition, a

good immunity to FNS and harmonics is observed under off-nominal frequency conditions. Therefore, it can be concluded that the proposed scheme is a potential technique for synchronization of single/three-phase grid connected power electronic equipment.

VII. Acknowledgment

The authors are thankful to Council of Scientific and Industrial Research, New Delhi, India for financial support (Ref. No. 22(0754)/17/EMR-II dated 10-10-2017).

References

[1] T. D. C. Busarello, A. Mortezaei, A. Péres, M. G. Simões, "Application of the conservative power theory current decomposition in a load power-sharing strategy among distributed energy resources," *IEEE Trans. Ind. Appl.*, vol. 54, no. 4, pp. 3771–3781, Mar. 2018.

[2] M. Aiello, A. Cataliotti, V. Cosentino, and S. Nuccio, "Synchronization techniques for power quality instruments," *IEEE Trans. Instrum. Meas.*, vol. 56, no. 5, pp. 1511–1519, Oct. 2007.

[3] S. Peyghami, H. Mokhtari, F. Blaabjerg, and Y. Yang, "Grid synchronization for distributed generations," *Encycl. Sus. Tech., Elsevier Sci.*, pp. 179–194, Oct. 2017.

[4] G. G. Talapur, H. M. Suryawanshi, L. Xu, and A. B. Shitole, "A reliable microgrid with seamless transition between grid connected and islanded mode for residential community with enhanced power quality," *IEEE Trans. Ind. Appl.*, vol. 54, no. 5, pp. 5246–5255, Sep./Oct. 2018.

[5] P. Shukl and B. Singh, "Grid integration of three-phase single-stage PV system using adaptive Laguerre filter based control algorithm under nonideal distribution system," *IEEE Trans. Ind. Appl.*, vol. 55, no. 6, pp. 6193–6202, Nov./ Dec. 2019.

[6] F. D. Freijedo, A. G. Yepes, O. Lopez, P. Fernandez-Comesana, and J. Doval-Gandoy, "An optimized implementation of phase locked loops for grid applications," *IEEE Trans. Instrum. Meas.*, vol. 60, no. 9, pp. 3110–3119, Sep. 2011.

[7] F. Chishti, S. Murshid, B. Singh, "Weak grid intertie WEGS with hybrid generalized integrator for power quality improvement," *IEEE Trans. Ind. Electron.*, vol. 67, no. 2, pp. 1113–1123, Feb. 2020.

[8] Y. Han, M. Luo, X. Zhao, J. M. Guerrero, and L. Xu, "Comparative performance evaluation of orthogonal-signal-generators-based single-phase PLL algorithms–A survey," *IEEE Trans. Power Electron.*, vol. 31, no. 5, pp. 3932–3944, May. 2016.

[9] M. Karimi-Ghartemani, S. A. Khajehoddin, P. K. Jain, and A. Bakhshai, "Derivation and design of in-loop filters in phase-locked loop systems," *IEEE Trans. Instrum. Meas.*, vol. 61, no. 4, pp. 930–940, Apr. 2012.

[10] S. Golestan, J. M. Guerrero and J. C. Vasquez, "Three-Phase PLLs: A Review of Recent Advances," *IEEE Trans Power Electron.*, vol. 32, no. 3, pp. 1894–1907, Mar. 2017.

[11] S. Golestan, J. M. Guerrero and J. C. Vasquez, "Single-Phase PLLs: A Review of Recent Advances," *IEEE Trans Power Electron.*, vol. 32, no. 12, pp. 9013–9030, Dec. 2017.

[12] S. Golestan, J. M. Guerrero, A. Vidal, A. G. Yepes, and J. Doval-Gandoy, "PLL With MAF-Based Prefiltering Stage: Small-Signal Modeling and Performance Enhancement," *IEEE Trans Power Electron.*, vol. 31, no. 6, pp. 4013–4019, Jun 2016.

[13] P. R.-Sánchez, X. D. T. García, A. P. Torres, and V. Feliu, "Fundamental positive- and negative-sequence estimator for grid synchronization under highly disturbed operating conditions," *IEEE Trans. Power Electron.*, vol. 28, no. 8, pp. 3733–3746, Aug. 2013.

[14] Y. Bai, X. Guo, B. Wang, and Y. Li, "Fully digital grid synchronization under harmonics and unbalanced conditions," *IEEE Access*, vol. 7, pp. 109969–109981, Aug. 2019.

[15] P. V. Bhansali and R. Potter, "Digital Demodulation," *IEEE Trans. Instrum. Meas.*, vol. IM-35, no. 3, pp. 324–327, Sept. 1986.

[16] C. A. G. Marques, M. V. Ribeiro, and E. A. B. Da Silva, "Enhanced demodulation-based technique for estimating the parameters of fundamental component in power systems," *IET Gener. Transm. Distrib.*, vol. 5, no. 9, pp. 979–988, Sep. 2011.

[17] I. Sadinezhad and V. G. Agelidis, "Frequency adaptive least-squares-Kalman technique for real-time voltage envelope and flicker estimation," *IEEE Trans. Ind. Electron.*, vol. 59, no. 8, pp. 3330–3341, Aug. 2012.

[18] P. Regulski and V. Terzija, "Estimation of frequency and fundamental power components using an unscented Kalman filter," *IEEE Trans. on Instrum. and Meas.*, vol. 61, no. 4, pp. 952–962, 2012.

[19] M. S. Reza, M. Ciobotaru, and V. G. Agelidis, "Differentiation filter-based technique for robust estimation of single-phase grid voltage frequency under distorted conditions," *IET Gener. Transm. Distrib.*, vol. 8, no. 5, pp. 907–915, May 2014.

[20] K. Mathuria, I. Hussain, B. Singh, and N. Kumar, "A quadrature oscillator-based DT for accurate estimation of fundamental load current for PV system in distribution network," *IEEE Trans. Ind. Informat.*, vol. 15, no. 6, pp. 3324–3333, Jun. 2019.

[21] F. D. Freijedo, J. D.-Gandoy, Ó. López, and E. Acha, "A generic open-loop algorithm for three-phase grid voltage/current synchronization with particular reference to phase, frequency, and amplitude estimation," *IEEE Trans. Power Electron.*, vol. 24, no. 1, pp. 94–107, Jan. 2009.

[22] M. Mirhosseini, J. Pou, V. G. Agelidis, E. Robles, and S. Ceballos, "A three-phase frequency-adaptive phase-locked loop for independent single-phase operation," *IEEE Trans. Power Electron.*, vol. 29, no. 12, pp. 6255–6259, Dec. 2014.

[23] Peng Liu, and Shanxu Duan, "An open-loop synchronization technique with simple structure for phase error compensation and frequency estimation," *IEEE Trans. on Ind. Electron.*, Early Access, 2019.

[24] A. K. Verma, R. K. Jarial, P. R.-Sánchez, U. M. Rao, and J. M. Guerrero, "An improved hybrid pre-filtered open-loop algorithm for three-phase grid synchronization," *IEEE Trans. on Ind. Electron.*, Early Access, 2020.

[25] P. A. Ioannou and J. Sun, *Robust adaptive control*. Upper Saddle River, N.J.: Prentice Hall, 1996.

[26] G. Tao, *Adaptive Control Design and Analysis*. Hoboken, N.J., USA: Wiley, 2003.

[27] M. Rahmani and I. Nodozi, "Phase-locked loops redesign by the lyapunov theory," *Electronics Letters*, vol. 51, no. 21, pp. 1664–1666, Oct. 2015.

[28] M. R. P. Ragazzon, M. G. Ruppert, D. M. Harcombe A. J. Fleming, and J. T. Gravdahl, "Lyapunov Estimator for High-Speed Demodulation in Dynamic Mode Atomic Force Microscopy," *IEEE Trans. Control Syst. Technol.*, vol. 26, no. 2, pp. 765–772, Mar. 2018.

[29] H. Ahmed and M. Benbouzid, "Demodulation type single-phase PLL with DC offset rejection," *Electronics Letters*, vol. 56, no. 7, pp. 344–347, Mar. 2020.

[30] *Voltage Characteristics of Electricity Supplied by Public Distribution Systems*, Eur. Std. EN 50160, 2008.

[31] R. G. Lyons, *Understanding digital signal processing*. Upper Saddle River, N. J.: Prentice Hall, 2011.

[32] *Testing and Measurement TechniquesGeneral Guide on Harmonics and Interharmonics Measurements and Instrumentation, for Power Supply Systems and Equipment Connected Thereto*, IEC Standard 61000–4–7, 2002.